

Reorientation transition in $\text{Fe}_n/\text{Au}(100)$

I. Reichl, A. Vernes, and P. Weinberger

Center for Computational Materials Science, Vienna University of Technology, Gumpendorferstr. 1a, A-1060 Vienna, Austria

L. Szunyogh

Department of Theoretical Physics and Center for Applied Mathematics and Computational Physics, Budapest University of Technology and Economics, Budafoki út 8, H-1521 Budapest, Hungary and Center for Computational Materials Science, Vienna University of Technology, Gumpendorferstr. 1a, A-1060 Vienna, Austria

C. Sommers

Laboratoire de Physique des Solides, Université de Paris-Sud 91405 Orsay Cedex, France

(Received 3 February 2005; published 22 June 2005)

Experimental investigations and theoretical magnetic anisotropy energy calculations show a reorientation transition of the magnetization in $\text{Fe}_n/\text{Au}(100)$ from a normal-to-plane to an in-plane direction at about three monolayers of Fe. In the present paper the magneto-optical properties of this system are investigated theoretically by using the spin-polarized relativistic screened Korringa-Kohn-Rostoker method, the Kubo-Greenwood equation for finite photon frequencies, and a classical optical approach that takes into account all reflections and interferences. By varying the thickness of the Fe film, the reorientation of the ground-state magnetization is clearly traced as a strong decrease in the calculated Kerr rotation angles for oblique incidence of light. For all film thicknesses under consideration, it is found that by continuously varying the angle of the incident light the Kerr rotation angle reaches a maximum at an incidence of about 70° . In the case of normal incidence a direct proportionality of the Kerr angles to the normal component of the magnetization is demonstrated by changing the orientation of the magnetization. When relating Kerr angles as calculated for a set of angles between the surface normal and the orientation of the magnetization to the corresponding magnetic anisotropy energy a very compact description of the occurring reorientation transition can be given. Moreover, based on these data and using a simple phenomenological picture a qualitative description of the Kerr angles with respect to applied external fields is provided.

DOI: 10.1103/PhysRevB.71.214416

PACS number(s): 77.22.Ch, 78.20.Bh, 78.20.Ci, 78.20.Ls

I. INTRODUCTION

Back in 1989 Liu and Bader¹ reported on an *in situ* surface magneto-optic Kerr effect (SMOKE) measurement for Fe on Au(100). They found sub-monolayer ferromagnetism, which, however, was unstable because of diffusion of Fe into the Au substrate and also because of Au segregation on top of the surface. Furthermore, they observed that the Fe/Au(100) system had no thermally stable out-of-plane easy axis in any thickness range. Grown at room temperature, Fe on Au(100) exhibited an in-plane easy axis in the monolayer regime; grown at 100 K, the easy axis turned out to be out-of-plane for films thinner than 2.8 monolayers (ML) and in-plane for thicker films. As a comparison will be made to these measurements, it seems appropriate to recall important experimental details of this by now famous study, namely (1) crossed magnetic fields (oriented in-plane and normal to the film plane) were used to sequentially monitor the corresponding magnetization components, whereby the in-plane and the normal-to-plane configurations were referred to as longitudinal and polar geometries, respectively; (2) a *p*-polarized He-Ne laser source was used; and (3) as analyzer served a crystal prism polarizer nearly crossed with the incident polarization. The experimental evidence for the reorientation transition can be summarized as follows: if the easy axis was in-plane, then the longitudinal SMOKE signal yielded a square hysteresis loop while the polar SMOKE

signal produced no hysteresis. If, however, the easy axis was normal to the film, then the polar SMOKE signal yielded a square hysteresis loop and the longitudinal SMOKE signal showed no hysteresis. In a regime of canted magnetization hysteresis, loops related to both configurations occurred. At a given film thickness the Kerr intensity was identified with the height of the hysteresis loop in the remanent state.

Using the spin-polarized relativistic screened Korringa-Kohn-Rostoker (KKR) method² the magnetic anisotropy energy E_a , defined as the sum of the band-energy anisotropy ΔE_b and the magnetic dipole-dipole interaction energy ΔE_{dd} , was calculated for $\text{Fe}_n/\text{Au}(100)$ and found a perpendicular orientation of the magnetization for $n \leq 3$ and an in-plane magnetization for $n \geq 4$.

In the present paper the magneto-optical properties of this system are investigated theoretically by varying not only the thickness of the Fe film, but also the geometry that relates the direction of the incoming light to the orientation of the magnetization.

A. Computational aspects

The charge and magnetization densities were calculated self-consistently for $\text{Fe}_n/\text{Au}(100)$, $n=1, \dots, 6$, in terms of the spin-polarized relativistic screened KKR method³ using the density functional parameterization of Vosko *et al.*⁴ and a

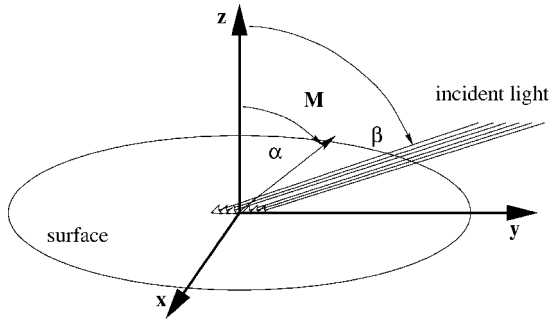


FIG. 1. The Kerr setup used in the calculations in the case of p -polarized incident light. Here α and β specify the orientation of the magnetization \mathbf{M} and the direction of the incident light, respectively. Both are specified with respect to the surface normal. Note that the magnetization always lies in the plane of incidence.

uniform perpendicular orientation of the magnetization. The corresponding potentials served then as input for the evaluation of the magneto-optical conductivity tensor.⁵ Both angles in Fig. 1, namely the orientation of the magnetization (α) and the incidence of light (β), were varied in steps of 5° between 0° and 90° . It should be noted, however, that the angle α is varied only for normal incidence of light ($\beta=0^\circ$) and that a scan over the angle β is performed only for the ground-state orientation of the magnetization ($\alpha=0^\circ$ or 90°).

Since for $\text{Fe}_n/\text{Au}(100)$ there are no experimental spectra of the Kerr rotation angle θ_K and ellipticity angle ε_K available in the literature, a photon energy of 3.8 eV was chosen that in the case of $(\text{Fe}_n\text{Au}_n)_N$ superlattices on a Au substrate yields simultaneously the largest experimentally detected θ_K and ε_K in the visible regime.⁶ For this particular photon energy the magneto-optical conductivity tensor was determined fully relativistically by using the approach discussed in detail in Ref. 5. The classical optical calculations were carried out then by means of the 2×2 matrix technique as described in Ref. 7 and the last entry in Ref. 5.

II. RESULTS

A. The permittivity of the top Fe layer

Kawagoe *et al.*⁸ measured the ratio of the amplitudes of the complex reflectivities for p - and s -polarized light, $\rho(\lambda)=R_p/R_s$ (λ being the wavelength), in the $\text{Fe}/\text{Au}(100)$ and $\text{Fe}/\text{Ag}(100)$. They varied the number of Fe layers from 2 to 20, used an optical wavelength regime of 270–760 nm (1.6–4.6 eV) and fixed the angle between the surface normal and the incident light to 57° . By taking into account multiple reflections and using the optical constants of bulk Au they then deduced an effective dielectric constant ε of the upper Fe layer in $\text{Fe}_8/\text{Au}(100)$: at a photon energy of 3.8 eV they obtained -3.68 and 9.82 for the real (ε') and imaginary (ε'') parts of ε , respectively. For the top Fe layer in $\text{Fe}_6/\text{Au}(100)$, the largest system investigated in here, the *ab initio* calculated values of -5.26 and -2.06 for ε'_{xx} and ε'_{zz} as well as 5.09 and 4.45 for ε''_{xx} and ε''_{zz} compare reasonably well with the experimental data and confirm *a posteriori* the procedure

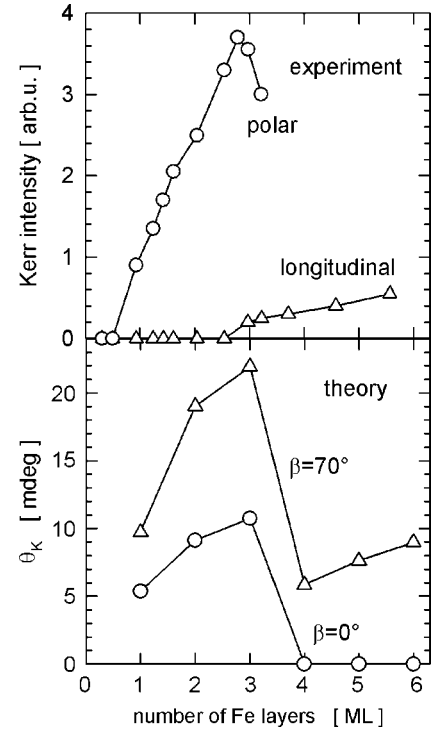


FIG. 2. Top: SMOKE experiments by Liu and Bader (Ref. 1). Circles denote the measured data for the polar, whereas triangles for the longitudinal Kerr setup. Bottom: calculated values of the Kerr rotation angle θ_K in the case of p -polarized incident light and for the magnetic ground state of $\text{Fe}_n/\text{Au}(100)$. Circles mark the theoretical results for a normal incidence ($\beta=0^\circ$) and triangles for an incidence of $\beta=70^\circ$ (see also Fig. 1).

adopted in Ref. 8. It should be noted that the calculated off-diagonal element is by one to two orders of magnitude smaller than the diagonal ones.

B. The magneto-optical Kerr effect in polar and longitudinal geometry

Since—as already stated—in the SMOKE experiments by Liu and Bader¹ the polar and longitudinal Kerr intensities are given by the height of the hysteresis loops in the remanent state, the reorientation transition from a perpendicular to an in-plane orientation of the magnetization is manifested in a strong decrease of the Kerr intensity for normal incidence ($\beta=0^\circ$) and a rather moderate increase of the Kerr intensity for grazing incidence ($\beta=90^\circ$) (see the upper part of Fig. 2). By considering the ground-state orientations of the magnetization resulting from magnetic anisotropy energy calculations the lower part of this figure shows the calculated Kerr rotation angles for two different angles of incidence, namely, for $\beta=0^\circ$ and 70° . Although Kerr angles and Kerr intensities cannot be directly related to each other, due to their linear dependence on the magnetization projected onto the direction of the incident light, it is not surprising at all that their respective dependence on the number of Fe layers is in good qualitative agreement. As can be immediately seen from Fig. 2, the calculated Kerr rotation angle for the system $\text{Fe}_n/\text{Au}(100)$ in the magnetic ground state remarkably well

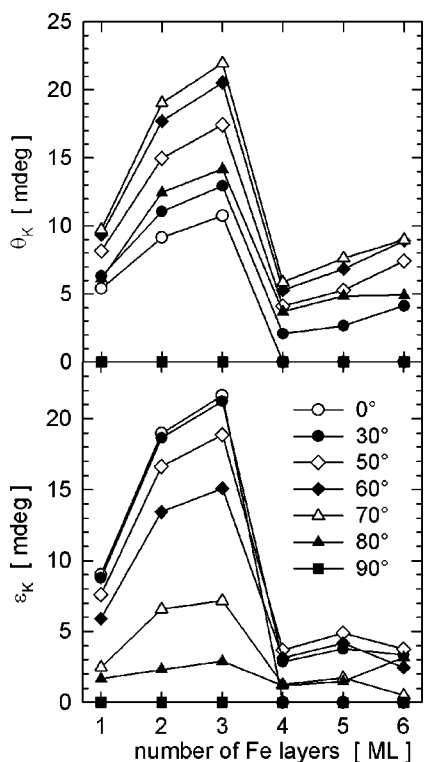


FIG. 3. The calculated Kerr rotation angle (upper part) and ellipticity angle (lower part) for different angles of incidence (see Fig. 1) for the corresponding magnetic ground state of $\text{Fe}_n/\text{Au}(100)$.

describes the magnetic reorientation transition in comparison with the experiments:¹ the perpendicular orientation of the magnetization is preferred below 3 ML, whereas above this Fe thickness the ground state is characterized by an in-plane orientation of the magnetization giving rise to exactly zero Kerr rotation angles for normal incidence. Since the present theoretical model does not include non-collinear magnetic arrangements, the reorientation transition⁹ (and consequently the calculated Kerr rotation angles) is not as smooth as in the experiment. In the case of oblique incidence (say for $\beta=70^\circ$) nonvanishing Kerr rotation angles are obtained for both normal-to-plane ($n \leq 3$) and in-plane ($n > 4$) ground-state magnetizations and the reorientation transition appears as a drop in θ_K . It is interesting to note that for $\beta=70^\circ$ the value of θ_K is by a factor of 2 to 3 larger than that for $\beta=0^\circ$ ($n \leq 3$).

C. The magneto-optic Kerr effect for arbitrary incidence of light and orientation of magnetization

For the magnetic ground state of $\text{Fe}_n/\text{Au}(100)$ the theoretical Kerr rotation angles θ_K and ellipticity angles ε_K are shown in Fig. 3 for oblique incidence of p -polarized light. Similar as in Fig. 2 (with exception of grazing incidence, $\beta=90^\circ$), all curves have a maximum at $n=3$ and—as a consequence of the reorientation transition—considerably decrease for $n=4$. For $n \leq 3$, i.e., for a normal-to-plane ground-state magnetization, the Kerr ellipticity angle continuously decreases as the angle of incidence β increases, a feature that does not apply for the Kerr rotation angle.

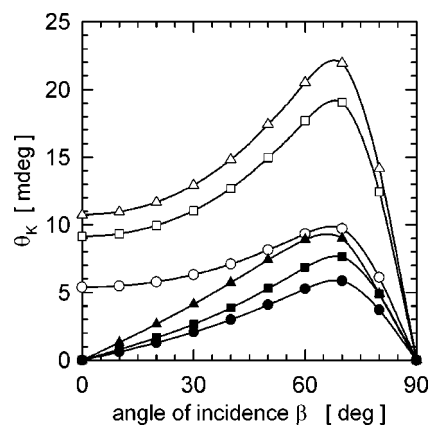


FIG. 4. The calculated Kerr rotation angle as a function of the angle of incidence β and for different thicknesses of Fe films on $\text{Au}(100)$. Open circles, squares, and triangles refer to 1, 2, and 3 ML of Fe on the top of $\text{Au}(100)$, respectively; full circles, squares, and triangles to 4, 5, and 6 ML, respectively.

As can be seen from Fig. 4 the Kerr rotation angle for oblique incidence increases independent of the Fe thickness until $\beta=70^\circ$, where a maximum of θ_K is reached; increasing the incidence angle β beyond 70° causes a continuous decrease of the Kerr rotation angle. It seems therefore that two regimes of $\theta_K(\beta)$ values can be distinguished: one for $n \leq 3$ ($\alpha=0^\circ$) where $\theta_K(\beta=0^\circ) \neq 0$, and one for $n > 4$ ($\alpha=90^\circ$) with $\theta_K(\beta=0^\circ)=0$.

For the particular case of $\text{Fe}_4/\text{Au}(100)$ the Kerr angles are displayed in Fig. 5 for normal incidence ($\beta=0^\circ$) and different orientations of the magnetization, $0 \leq \alpha \leq 90^\circ$. As can be seen from this figure both $\theta_K(\alpha)$ and $\varepsilon_K(\alpha)$ show an almost perfect $\cos(\alpha)$ dependence. This finding supports the experimentally known fact that for normal incidence the Kerr rotation angle is directly proportional to the normal component of the magnetization.

D. Kerr angles versus magnetic anisotropy energies

For the case of normal incidence Fig. 6 offers an interesting view of the Kerr angles, $\theta_K(\alpha)$ and $\varepsilon_K(\alpha)$, since in this figure each entry refers to a particular value of α , the ab-

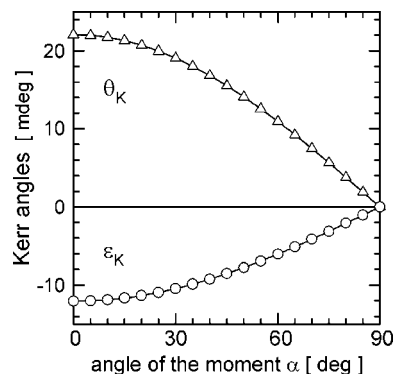


FIG. 5. The calculated Kerr angles in the case of normal incidence for $\text{Fe}_4/\text{Au}(100)$ as a function of the angle α (see Fig. 1).

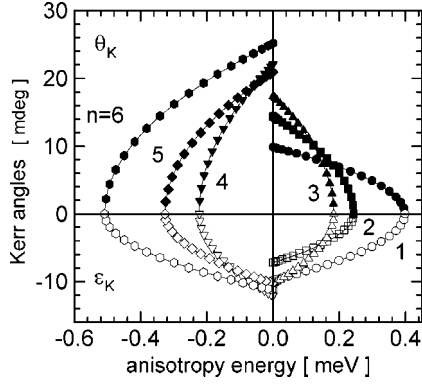


FIG. 6. The calculated Kerr angles displayed as a function of the magnetic anisotropy energy for different thicknesses of the Fe film on Au(100). Full symbols refer to Kerr rotation, open symbols to Kerr ellipticity angles. The data for this figure were obtained by varying the angle of magnetization α while the angle of incidence is fixed to $\beta=0^\circ$ (see Fig. 1).

scissa being the anisotropy energy $E_a(\alpha)$. Obviously points along the ordinate ($E_a=0$) correspond to $\alpha=90^\circ$, while those along the abscissa belong to $\alpha=0^\circ$. For $n \leq 3$ all curves fall into the regime of positive anisotropy energies (perpendicular orientation of the magnetization), while those for $n \geq 4$ refer to that of negative anisotropy energies (in-plane orientation). The reorientation transition is thus particularly clearly visualized.

The paths shown in Fig. 6 can, in principle, be accessed experimentally if continuous reorientation transitions are induced by applying external magnetic fields in appropriate directions. Assuming a second-order anisotropy, $E_a(\alpha) = -K \cos^2(\alpha)$, for the case of $K > 0$ (perpendicular anisotropy) a longitudinal magnetic field yields the equilibrium orientations,

$$\alpha = \begin{cases} 90^\circ & \text{for } H > H_0, \\ \arcsin(H/H_0) & \text{for } -H_0 < H \leq H_0, \\ -90^\circ & \text{for } H \leq -H_0 \end{cases} \quad (1)$$

where $H_0 = 2K/M$ and M is the (total) magnetic moment of the ferromagnetic system. In the case of an in-plane anisotropy ($K < 0$) a polar magnetic field has to be applied in order to induce a continuous reorientation transition,

$$\alpha = \begin{cases} 0^\circ & \text{for } H > H_0, \\ \arccos(H/H_0) & \text{for } -H_0 < H \leq H_0, \\ 180^\circ & \text{for } H \leq -H_0 \end{cases} \quad (2)$$

with $H_0 = -2K/M$.

In Fig. 7 exactly the same Kerr angles as in Fig. 6 are used, but this time as a function of an applied external magnetic field, the size of which being obtained by using either Eq. (1) ($n \leq 3$) or Eq. (2) ($n > 3$). Clearly enough it is sufficient to depict only the corresponding curves for $H > 0$. Since, as shown before, Kerr angles are directly proportional to $\cos(\alpha)$, it is not surprising that within the range of $|H| \leq H_0$ for $K > 0$ the Kerr rotation angles in Fig. 7 follow the relation below:

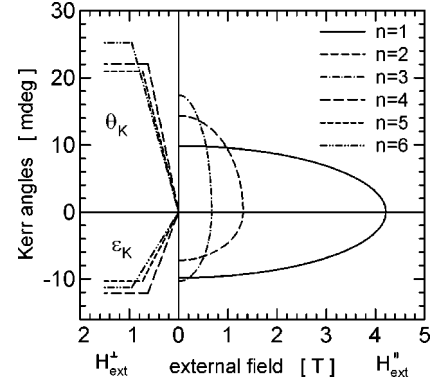


FIG. 7. The calculated Kerr angles displayed as a function of a longitudinal ($H_{\text{ext}}^{\parallel}$, right part) and a polar (H_{ext}^{\perp} , left part) external magnetic field applied to $\text{Fe}_n/\text{Au}(100)$ for $n \leq 3$ and $n > 4$, respectively. As in Fig. 6 the data for this figure were obtained by varying α and keeping the angle of incidence fixed to $\beta=0^\circ$ (see also Fig. 1).

$$\theta_K = \theta_{K0} \sqrt{1 - (H/H_0)^2}, \quad (3)$$

where θ_{K0} denotes the Kerr rotation angle for vanishing external field, and for $K < 0$

$$\theta_K = \theta_{K0} \frac{H}{H_0}, \quad (4)$$

where θ_{K0} now refers to the Kerr rotation angle at H_0 . Similar expressions apply for the ellipticity angles. It should be noted that the obtained values of H_0 are typically by one order of magnitude larger than the experimentally measured coercive fields,¹ which within the model used here are equivalent to H_0 .

III. CONCLUSION

The present calculations illustrate in quite some detail the change of the magneto-optical properties near and at a reorientation transition and thus most likely provide a clearer view of what exactly is mapped in Kerr measurements when the thickness of the magnetic film is changed and when the polar Kerr effect does not apply. In particular Fig. 6 provides a compact view of the relationship between Kerr quantities and the anisotropy energy. Furthermore, by associating non-equilibrium canted magnetic states with applied external fields along appropriate directions, it is possible to characterize in a very simple manner Kerr angles as functions of these fields.

ACKNOWLEDGMENTS

Financial support from Austrian Ministries (GZ 45.531, ZI 98.366, CONEX II), the Austrian Science Foundation (W004), the Wissenschaftlich-Technisches Abkommen Austria-Hungary (A-3/03), and the Hungarian National Science Foundation (OTKA T037856, T046267) are gratefully acknowledged.

- ¹C. Liu and S. D. Bader, *J. Vac. Sci. Technol. A* **8**(3), 2727 (1990).
- ²L. Szunyogh, B. Újfalussy, and P. Weinberger, *Phys. Rev. B* **51**, 9552 (1995).
- ³J. Zabloudil, R. Hammerling, L. Szunyogh, and P. Weinberger, *Electron Scattering in Solid Matter* (Springer Verlag, Heidelberg, 2004).
- ⁴S. H. Vosko, L. Wilk, and M. Nusair, *Can. J. Phys.* **58**, 1200 (1980).
- ⁵L. Szunyogh and P. Weinberger, *J. Phys.: Condens. Matter* **11**, 10451 (1999); A. Vernes, L. Szunyogh, and P. Weinberger, *ibid.* **13**, 1529 (2001); A. Vernes, L. Szunyogh, and P. Weinberger, *Phys. Rev. B* **65**, 144448 (2002); A. Vernes, L. Szunyogh, and P. Weinberger, *ibid.* **66**, 214404 (2002); A. Vernes, I. Reichl, P. Weinberger, L. Szunyogh, and C. Sommers, *ibid.* **70**, 195407 (2004); I. Reichl, R. Hammerling, A. Vernes, P. Weinberger, C. Sommers, and L. Szunyogh, *ibid.* **70**, 214417 (2004); A. Vernes and P. Weinberger, *ibid.* **70**, 134411 (2004).
- ⁶K. Takanashi, S. Mitani, H. Fujimori, K. Sato, and Y. Suzuki, *J. Magn. Magn. Mater.* **177-181**, 1199 (1998).
- ⁷I. Reichl, A. Vernes, C. Sommers, L. Szunyogh, and P. Weinberger, *Philos. Mag.* **84**, 2543 (2004).
- ⁸T. Kawagoe, K. Nakamura, T. Terashima, H. Kaihoko, and T. Mizoguchi, *J. Magn. Magn. Mater.* **148**, 185 (1995).
- ⁹L. Udvardi, R. Király, L. Szunyogh, F. Denat, M. B. Taylor, B. L. Györfy, B. Újfalussy, and C. Uiberacker, *J. Magn. Magn. Mater.* **183**, 283 (1998); L. Udvardi, L. Szunyogh, A. Vernes, and P. Weinberger, *Philos. Mag. B* **81**, 613 (2001).